Feed-Forward Bullet-Time Reconstruction of Dynamic Scenes from Monocular Videos

Hanxue Liang[1,2]*, **Jiawei Ren**[1,3]*, **Ashkan Mirzaei**[1,4]*, **Antonio Torralba**[1,5],
Ziwei Liu[3], **Igor Gilitschenski**[4], **Sanja Fidler**[1,4,6],
Cengiz Oztireli[2], **Huan Ling**[1,4,6], **Zan Gojcic**[1]†, **Jiahui Huang**[1]†

[1]NVIDIA, [2]University of Cambridge, [3]Nanyang Technological University,
[4]University of Toronto, [5]MIT, [6]Vector Institute
https://research.nvidia.com/labs/toronto-ai/bullet-timer/

Abstract

Recent advancements in static feed-forward scene reconstruction have demonstrated significant progress in high-quality novel view synthesis. However, these models often struggle with generalizability across diverse environments and fail to effectively handle dynamic content. We present BTimer (short for BulletTimer), **the first motion-aware feed-forward model for real-time reconstruction and novel view synthesis of dynamic scenes**. Our approach reconstructs the full scene in a 3D Gaussian Splatting representation at a given target ('bullet') timestamp by *aggregating* information from all the context frames. Such a formulation allows BTimer to gain scalability and generalization by leveraging both static and dynamic scene datasets. Given a casual monocular dynamic video, BTimer reconstructs a *bullet-time*[1] scene within 150ms on 256 × 256 resolution while reaching state-of-the-art performance on both static and dynamic scene datasets, even compared with optimization-based approaches.

1 Introduction

Multi-view reconstruction and novel-view synthesis are long-standing challenges in computer vision, with numerous applications ranging from AR/VR to simulation and content creation. While significant progress has been made in reconstructing static scenes, dynamic scene reconstruction from monocular videos remains challenging due to the inherently ill-posed nature of reasoning about dynamics from limited observations [2].

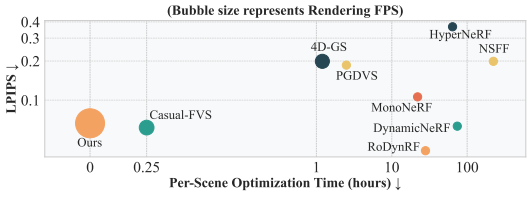

Figure 1: **Rendering quality vs. speed.** Our model can reconstruct and render dynamic scenes at a much faster speed than existing approaches with a competitive quality. Numbers are reported on NVIDIA Dynamic Scene Dataset [1]

Current methods for static scene reconstruction can be broadly divided into two categories: optimization-based [3, 4] and feed-forward [5, 6] approaches. However, extending both of these to *dynamic scenes* is not straightforward. To reduce the ambiguities of scene dynamics, many optimization-based methods aim to constraint the problem with data priors such as depth and

*/†: Equal contribution/advising.

[1]In this paper, we define *bullet-time* as the instantiation of a 3D scene *frozen* at a given/fixed timestamp t.

39th Conference on Neural Information Processing Systems (NeurIPS 2025).

optical flow [2, 7, 8, 9]. However, balancing these priors with the data remains challenging [10, 11]. Moreover, per-scene optimization is time-consuming and thus difficult to scale.

On the other hand, to avoid the lengthy per-scene-optimization, recent feed-forward approaches [12, 13, 14, 15, 16, 5] explored learning generalizable models on large-scale datasets to directly perform static scene reconstructions, thereby learning strong priors from data. These inherent priors could help resolve ambiguities due to complex motion, but none of previous approaches have yet been extended to dynamic scenes. This limitation stems from both the complexity of modeling dynamic scenes and the lack of 4D supervision data. The only feed-forward dynamic reconstruction model [17] is thus trained on synthetic object-centric datasets, requires fixed camera viewpoints and multiview supervision, and cannot generalize to real-world scene scenarios.

In this work, we aim to answer the question: *How can one build a feed-forward reconstruction model that can handle dynamic scenes effectively?* We build upon the recent success of the pixel-aligned 3D Gaussian Splatting (3DGS [18]) prediction models [5] and propose a novel *bullet-time* formulation for feed-forward dynamic reconstruction. The core idea is simple yet effective: we add a *bullet-time* embedding to the context (input) frames, indicating the desired timestamp for the output 3DGS representation. Our model is trained to aggregate the predictions of context frames to reflect the scenes at the *bullet* timestamp, yielding a spatially complete 3DGS scene. This design not only naturally unifies the static and dynamic reconstruction scenarios, but also enables our model to become implicitly motion-aware while learning to capture scene dynamics. In particular, the proposed formulation **(i)** allows us to pre-train our model on large amounts of *static* scene data, **(ii)** scales effectively across datasets, without being constrained by duration and frame rates of input videos, and **(iii)** outputs volumetric video representations that inherently support multiple viewpoints. Meanwhile, in the presence of fast motions, we additionally introduce a Novel Time Enhancer (NTE) module to predict the intermediate frames before feeding them to the main model.

In summary, we present BTimer, *the first feed-forward model for real-time reconstruction and novel view synthesis of dynamic scenes.* To achieve this goal, we introduce the core bullet-time formulation and develop a curriculum training strategy that enables the learning of a highly generalizable model on a large, carefully curated dataset comprising both static and dynamic scenes. Furthermore, we present an additional NTE module to effectively handle fast motions, enhancing the model's robustness in challenging scenarios. Our method is highly efficient: feed-forward inference with 12 context frames of 256×256 resolution only costs 150ms on a single GPU, and the output 3DGS can be rendered in real-time. BTimer is capable of handling both static and dynamic reconstructions. It achieves competitive results on various reconstruction benchmarks, even surpassing many expensive per-scene optimization-based methods, as illustrated in Fig. 1.

2 Related work

Dynamic 3D representations. Depending on the tasks at hand, typical choices of 3D representations include voxels [19, 20], implicit fields/NeRFs [21, 3, 22], and point clouds/3D Gaussians [23, 18]. Representing dynamics on top has an even larger design space: One existing line of works directly builds a '4D' representation to enable feature queries at arbitrary positions and timestamps from an implicit field [24, 25] or via marginalization at a given step [26, 27], with the extensibility to higher dimensions such as material [28]. Another line of work first defines a canonical 3D space, and learns a deformation field to warp the canonical space to the target frame. While these methods learn additional information about shape correspondences, their performance heavily relies on the quality and topology of the canonical space.

Dynamic novel view synthesis. For tasks that require a relatively smaller view extrapolation, the problem of novel view synthesis can be tackled without explicit 3D geometry in the loop, using depth warping [1] or multi-plane images [29]. Otherwise, the study of novel view synthesis of dynamic scenes [30, 4] is mainly on (1) effectively optimizing the 3D representation through input images through monocular cues [31, 8, 11, 10] or geometry regularizations [32, 33], and (2) being able to render fast with grids [34], local-planes [35], or dynamic 3D Gaussians [36] formulation. Our method aims to provide a dynamic representation that is fast to build within hundreds of milliseconds while reaching competitive rendering quality as the above optimization-based methods.

Feed-forward reconstruction models. In many applications where the reconstruction speed is crucial, most optimization-based reconstruction methods become less preferable. To this end,one line

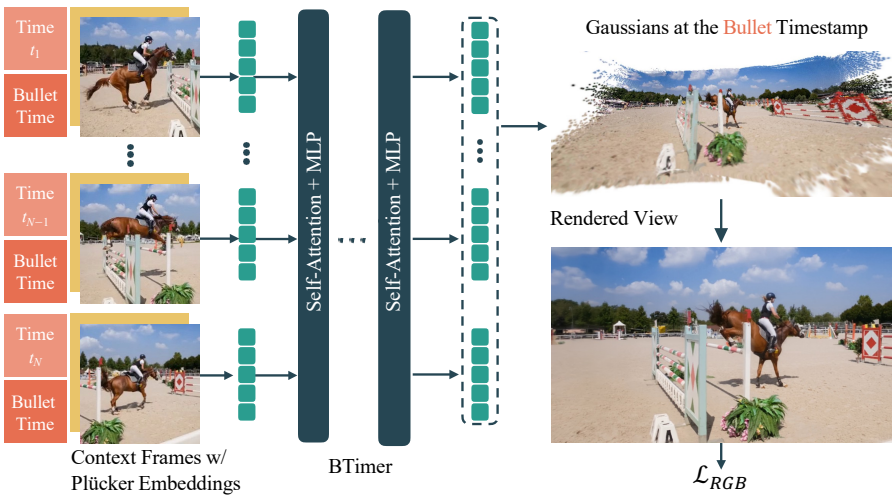

Figure 2: **BTimer.** The model takes as input a sequence of context frames and their Plücker embeddings, along with the context timestamp and target ('bullet') timestamp embeddings. It then directly predicts the 3DGS representation at the bullet timestamp.

of work that starts to emerge is fully feed-forward models that directly regress from 2D images to 3D, represented as either neural field [13, 37], triplanes [12], 3D Gaussians [14, 5, 15], sparse voxels [38], or latent tokens [16]. Crucially, while feed-forward reconstruction models for static scenes have seen development, the extension to dynamic scenes is still challenging. Existing methods either require hard-to-acquire consistent video depth as input [39], do not support rendering [40], or only work on object-scale data [17]. In contrast, our method supports reconstructing from a monocular video containing dynamic scenes in a fully feed-forward manner, and is able to render at arbitrary viewpoints and timestamps.

3 Method

Overview. Given a monocular video (image sequence) represented by $\mathcal{I} = \{\mathbf{I}_i \in \mathbb{R}^{H\times W\times 3}\}_{i=1}^N$ with N frames of width W and height H, along with known camera poses $\mathcal{P} = \{\mathbf{P}_i \in \mathbb{SE}(3)\}_{i=1}^N$, intrinsics, and corresponding timestamps $\mathcal{T} = \{t_i \in \mathbb{R}\}_{i=1}^N$, our goal is to build a feed-forward model capable of rendering high-quality novel views at arbitrary timestamps $t \in [t_1, t_N]$.

The core of our approach is a transformer-based *bullet-time* reconstruction model, named **BTimer**, that takes in a subset of frames $\mathcal{I}_c \subset \mathcal{I}$ (denoted as *context frames*) along with their corresponding poses $\mathcal{P}_c \subset \mathcal{P}$ and timestamps $\mathcal{T}_c \subset \mathcal{T}$, and outputs a complete 3DGS [18] scene frozen at a specified *bullet* timestamp $t_b \in [\min_{\mathcal{T}_c}, \max_{\mathcal{T}_c}]$ (§ 3.1). Iterating over all $t_b \in \mathcal{T}$ results in a full video reconstruction represented by a sequence of 3DGS. We further introduce a Novel Time Enhancer (NTE) module that synthesizes interpolated frames with timestamps $t \notin \mathcal{T}$ (§ 3.2). The output of the NTE module is used along with other context views as input to the bullet-time model to enhance reconstruction at arbitrary intermediate timestamps. To effectively train our model, we carefully design a learning curriculum (§ 3.3) that incorporates a large mixture of datasets containing both static and dynamic scenes, to enhance motion awareness and temporal consistency of our models.

3.1 BTimer reconstruction model

Model design. Inspired by [5], our BTimer model uses a ViT-based [41] network as its backbone, consisting of 24 self-attention blocks with LayerNorms [42] applied at both the beginning and the end of the model. We divide each input context frame $\mathbf{I}_i \in \mathcal{I}_c$ into 8×8 patches, which are projected into feature space $\{\mathbf{f}_{ij}^{\text{rgb}}\}_{j=1}^{HW/64}$ using a linear embedding layer. The camera Plücker embeddings [43] derived from the camera poses $\mathbf{P}_i \in \mathcal{P}_c$ and the time embeddings (detailed later) are processed similarly to form the camera pose features $\{\mathbf{f}_{ij}^{\text{pose}}\}$ and the time features $\{\mathbf{f}_i^{\text{time}}\}$ (shared for all patches j). These features are added together to form the input tokens for the patches of the context

frame $\{\mathbf{f}_{ij}\}_{j=1}^{HW/64}$, where $\mathbf{f}_{ij} = \mathbf{f}_{ij}^{\text{rgb}} + \mathbf{f}_{ij}^{\text{pose}} + \mathbf{f}_{i}^{\text{time}}$. The input tokens from all context frames are concatenated and fed into the Transformer blocks.

Each corresponding output token $\mathbf{f}_{ij}^{\text{out}}$ is decoded into 3DGS parameters $\mathbf{G}_{ij} \in \mathbb{R}^{8\times8\times12}$ using a single linear layer. Each 3D Gaussian is paramaterized by its RGB color $\mathbf{c} \in \mathbb{R}^3$, scale $\mathbf{s} \in \mathbb{R}^3$, rotation represented as unit quaternion $\mathbf{q} \in \mathbb{R}^4$, opacity $\sigma \in \mathbb{R}$, and ray distance $\tau \in \mathbb{R}$, resulting in 12 paramaters per Gaussian. The 3D position of each Gaussian $\boldsymbol{\mu} \in \mathbb{R}^3$ is obtained through pixel-aligned unprojection as $\boldsymbol{\mu} = \mathbf{o} + \tau\mathbf{d}$, where $\mathbf{o} \in \mathbb{R}^3$ and $\mathbf{d} \in \mathbb{R}^3$ are the ray origin and direction obtained from $\mathbf{P}_i$.

Time embeddings. The aforementioned input time feature $\mathbf{f}_i^{\text{time}}$ is obtained from: **(i) context** timestamp t_i that is separate for each context frame $\mathbf{I}_i$, and **(ii) bullet** timestamp t_b that is shared across all context frames i. Both timestamp scalars are encoded using standard Positional Encoding (PE) [44] with sinusoidal functions, and then passed through two linear layers to obtain the features $\mathbf{f}_i^{\text{ctx}}$ and $\mathbf{f}_i^{\text{bullet}}$ respectively. Finally, we set $\mathbf{f}_i^{\text{time}} = \mathbf{f}_i^{\text{ctx}} + \mathbf{f}_i^{\text{bullet}}$.

Supervision loss. Our model is supervised only by losses defined in the RGB image space, bypassing the need for any source of 3D ground truth that is hard to obtain for real data. The final loss is a weighted sum of Mean Squared Error (MSE) loss and Learned Perceptual Image Patch Similarity (LPIPS) [45] loss between the images rendered from the 3DGS output and the ground-truth image:

$$\mathcal{L}_{\text{RGB}} = \mathcal{L}_{\text{MSE}} + \lambda\mathcal{L}_{\text{LPIPS}}, \tag{1}$$

with $\lambda = 0.5$.

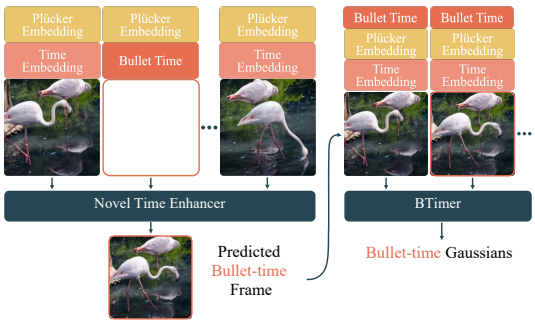

Figure 3: **NTE Module.** It takes as input the target bullet time embedding, target pose, as well as adjacent frames to directly predict corresponding RGB values. The predicted frame is then used in BTimer as *bullet* frame for novel time reconstruction.

Careful selection of input context frames and corresponding supervision frames (at the bullet timestamp) during training is essential for stable training and good convergence. In practice, we find the combination of the following two strategies particularly effective: **(i) In-context Supervision** where the supervision timestamp is randomly selected from the context frames, encouraging the model to accurately localize and reconstruct the context timestamps. For multi-view video datasets, images from additional viewpoints can also contribute to the loss. **(ii) Interpolation Supervision** where the supervision timestamp lies between two adjacent context frames. This forces the model to interpolate the dynamic parts while maintaining consistency for the static regions. The interpolation supervision significantly impacts our final performance (*cf*. § 4.4 for details); without it, the model falls into a local minima by positioning the 3D Gaussians close to the context views but hidden from other views.

Inference. Our *bullet-time* formulation makes it straightforward to reconstruct a full video, which only involves iteratively setting the bullet timestamp t_b to every single timestamp in the video, and can be done efficiently in parallel. For a video longer than the number of training context views $|\mathcal{I}_c|$, at timestamp t, apart from including this exact timestamp and setting $t_b = t$, we uniformly distribute the remaining $|\mathcal{I}_c| - 1$ required context frames across the whole duration of the video to form the input batch with $|\mathcal{I}_c|$ frames.

3.2 Novel time enhancer (NTE) module

While our BTimer model can already reconstruct the 3DGS representation for all observed timestamps, we notice that forcing it to reconstruct at a novel intermediate timestamp, *i.e*. performing interpolation at $t_b \notin \mathcal{T}$, leads to suboptimal results. In such cases, the exact bullet-time frame cannot be included in the context frames as it does not exist. Our model specifically fails to predict a smooth transition between adjacent video frames when the motion is complex and fast. This is mainly caused by the inductive bias of pixel-aligned 3D Gaussian prediction. To mitigate this issue, we propose a *3D-free* Novel Time Enhancer (NTE) module that directly outputs images at given timestamps, which are then used as input to our BTimer model, as illustrated in Fig. 3.

NTE module design. The design of this module is largely inspired by the very recent decoder-only LVSM [16] model. Specifically, NTE copies the same ViT architecture from the BTimer model, but the time features of input context tokens only encode their corresponding context timestamps (*i.e*. we set $\mathbf{f}_i^{\text{time}} = \mathbf{f}_i^{\text{ctx}}$). Additionally, we concatenate extra target tokens to the input tokens, which encode the target timestamp and the target pose for which we want to generate the RGB image. Following [16], we use QK-norm to stabilize training. Implementation-wise we apply an attention mask that masks all the attention to the target tokens, so KV-Cache (*cf*. [46]) can be used for faster inference. From the output of the Transformer backbone, we only retain the target tokens, which we then unpatchify and project to RGB values at the original image resolution using a single linear layer. The interpolation model is trained with the same objective as the main BTimer model (see § 3.1), but the output image is directly decoded from the network and not rendered from a 3DGS representation.

Integration with BTimer. While the NTE module can be used on its own to generate novel views, we empirically find the novel-*view*-synthesis quality to be inferior (§ 4.4). We hence propose to integrate it with our main BTimer model. To reconstruct a bullet-time 3DGS at $t_b \notin \mathcal{T}$, we first use NTE to synthesize $\mathbf{I}_b$ at the timestamp t_b, where the target pose $\mathbf{P}_b$ is linearly interpolated from the nearby context poses in $\mathcal{P}$, and the context frames are chosen as the nearest frames to t_b. To accelerate the inference of the interpolation model, we use the KV-Cache strategy. In practice we observe that the interpolation model adds negligible overhead to the overall runtime.

3.3 Curriculum training at scale

One important lesson people have learned from training deep neural networks is to scale up the training [47, 48], and the model's generalizability is largely determined by the data diversity. Since our bullet-time reconstruction formulation naturally supports both static (by equalizing all elements in $\mathcal{T}$) and dynamic scenes, and requires only RGB loss for weak supervision, we unlock the potential of leveraging the availability of numerous static datasets to pretrain our model. We hence aim to train a *kitchen-sink* reconstruction model that is *not specific* to any dataset, making it generalizable to both static and dynamic scenes, and capable of handling objects as well as both indoor and outdoor scenes. This is in contrast to, *e.g*., GS-LRM [5] or MVSplat [14] where one needs different models in different domains.

Notably, we apply the following training curriculum to BTimer and the NTE module separately, but during inference they are used jointly as explained in § 3.2.

Stage 1: Low-res to high-res static pretraining. To obtain a more generalizable 3D prior as initialization, we first pretrain the model with a mixture of *static* datasets. Time embedding will not be used in this stage. The collection of datasets covers object-centric (Objaverse [49]) and indoor/outdoor scenes (RE10K [50], MVImgNet [51], DL3DV [52]). The datasets cover both the synthetic and real-world domains and consist of 390K training samples. We normalize the scales of different datasets to be bounded roughly in a 10^3 cube. Due to the complex data distribution, our training starts from a low-resolution few-view setting that reconstructs on 128×128 resolution from $|\mathcal{I}_c| = 4$ context views. To further increase the reconstruction details, we fine-tune the model from 128×128 by first increasing the image resolution to 256×256, and then fine-tune to 512×512.

Stage 2: dynamic scene co-training. After the training on static scenes, we start fine-tuning the model along with time embedding projection layers on dynamic scenes with available 4D data that contains monocular or multi-view synchronized videos. We leverage Kubric [53], PointOdyssey [54], DynamicReplica [55] and Spring [56] datasets for training. Due to the scarcity of 4D data, during this stage we keep the static datasets for co-training which provides more multi-view supervision and stabilizes the training. Additionally, we build a customized pipeline to label the camera poses from Internet videos (detailed below), and add them to our training set to further enhance the model's robustness towards real-world data.

Stage 3: long-context window fine-tuning. Including more context frames is vital when reconstructing long videos. Therefore, as a final stage, we increase the number of context views from $|\mathcal{I}_c| = 4$ to $|\mathcal{I}_c| = 12$ to cover more frames. Note that this stage does not apply to NTE as it only takes nearby frames as input.

Annotating internet videos. We randomly select a subset from the PANDA-70M [57] dataset, and cut the videos into short clips with $\sim$20 s duration. We mask out the dynamic objects in the videos with Segment Anything Model [58] and then apply DROID-SLAM [59] to estimate the camera poses.

Model	Rec. Time	PSNR↑	SSIM↑	LPIPS↓
TiNeuVox [63]	0.75 h	14.03	0.502	0.538
NSFF [2]	24 h	15.46	0.551	0.396
T-NeRF [64]	12 h	16.96	0.577	0.379
Nerfies [32]	24 h	16.45	0.570	0.339
HyperNeRF [4]	72 h	16.81	0.569	0.332
PGDVS [39]	3 h†	15.88	0.548	0.340
Depth Warp	–	7.81	0.201	0.678
BTimer (**Ours**)	0.98 s	16.52	0.570	0.338

(a)

Model	Rec. Time	Render FPS	PSNR↑	LPIPS↓
HyperNeRF [4]	64 h	0.40	17.60	0.367
DynNeRF [65]	74 h	0.05	26.10	0.082
RoDynRF [33]	28 h	0.42	25.89	0.065
4D-GS [66]	1.2 h	44	21.45	0.199
Casual-FVS [9]	0.25 h	48	24.57	0.081
PGDVS [39]	3 h†	0.70	24.41	0.186
Depth Warp	–	–	12.63	0.564
BTimer (**Ours**)	0.78 s	115	25.82	0.086

(b)

Table 1: **Quantitative comparisons on dynamic datasets.** (a) DyCheck iPhone dataset [64] comparison. (b) NVIDIA Dynamic Scene dataset [1] comparison. The results are rendered on 480×270 resolution. 'Rec. Time' is per-scene reconstruction time. †: Video-consistent depth estimation step included. We highlight the best, second best, and third best results.

Low-quality videos or annotated poses are filtered out by measuring the reprojection error. The final dataset contains more than 40K clips with high-quality camera trajectories.

4 Experiments

In this section we first introduce necessary implementation details in § 4.1. We evaluate the performance of BTimer extensively on available dynamic scene benchmarks § 4.2, and demonstrate its *backward* compatibility with static scenes § 4.3. Ablation studies are found in § 4.4.

4.1 Implementation details

Training. Our backbone Transformer network is implemented efficiently with FlashAttention-3 [60] and FlexAttention [61]. We use `gsplat` [62] for robust and scalable 3DGS rasterization since the total number of 3D Gaussians generated by our model can be very large. For BTimer, the numbers of training iterations are fixed to 90K, 90K, and 50K for **Stage 1** training on 128^2, 256^2, and 512^2 resolutions, and are 10K and 5K for **Stage 2** and **Stage 3** dynamic scene training respectively. We use the initial learning rates of 4×10^{-4}, 2×10^{-4} and 1×10^{-4} for the three stages, and apply a cosine annealing schedule to smoothly decay the learning rate to zero. Training is conducted on 32 NVIDIA A100 GPUs. The learning rate, training GPU numbers and training schedules mainly follow [16, 5]. Training cost analysis and ablation on batch size can be found in the Supplement. We use the same training strategy for NTE. The numbers of iterations are 140K, 60K, and 30K for the progressive training in **Stage 1**, and are 20K for **Stage 2**, with the same learning rate schedule as above. As introduced in § 3.3, we use a mixture of multiple datasets for training [49, 51, 50, 52, 53, 54, 55, 56] along with our 40K annotated dataset on PANDA-70M [57]. Note that we make sure that none of the testing scenes we show below is included in the training datasets.

Inference cost. Our model can be flexibly applied to different resolutions and numbers of context views. Measured on a single NVIDIA A100 GPU, BTimer takes 20 ms for 4-view 256^2 reconstruction, 150 ms for the same resolution with 12 views, and 1.55 s for 12-view 512^2 reconstruction. It requires less than 10 GB memory, which easily fits on a commercial-grade GPU (Result shown in Supplement). Please note that our model inference can be parallelized and the overall time overhead remains constant given sufficient memory.

4.2 Dynamic novel view synthesis

4.2.1 Quantitative analysis

We provide quantitative evaluations on two of the largest dynamic view synthesis benchmarks.

DyCheck benchmark [64]. The benchmark includes a dataset that contains 7 dynamic scenes recorded by 3 synchronized cameras. Following the protocol in [64], we take images from the iPhone camera as our context frames and use the frames from the 2 other stationary cameras for evaluation (totaling 3928 images of resolution 360×480). Our baselines include per-scene optimization-based methods, *i.e.*, TiNeuVox [63], NSFF [2], T-NeRF [64], Nerfies [32] and HyperNeRF [4]. We additionally compare to a pseudo-feed-forward approach PGDVS [39].

Figure 4: **Visualizations on DAVIS dataset [67].** We show our renderings on novel combinations of view poses and timestamps, with the correspondending references shown on the left. The lower-left/right corner shows the rendered depth map for each example.

Figure 5: **Qualitative results** on DyCheck [65] (left) and NVIDIA dynamic scene [1] (right) benchmarks.

We report masked Peak Signal-to-Noise Ratio (PSNR), Structural Similarity Index Measure (SSIM) [68], and LPIPS following the benchmark protocol [64] in Tab. 1a, and show visualizations in Fig. 5. Note that since multi-frame inference can run in parallel, for our model we report single-frame reconstruction time regardless of video lengths. It is encouraging to observe that even without per-scene optimization, BTimer achieves a very competitive performance compared to the baselines, ranking 2$^{\text{nd}}$ in both SSIM and LPIPS scores. Our model surpasses PGDVS across all 3 metrics without the need of consistent depth estimate. This demonstrates our model's efficiency and strong generalization capability, being capable of providing sharper details and richer textures.

NVIDIA dynamic scene benchmark [1]. NVIDIA Dynamic Scene dataset contains 9 scenes captured by 12 forward-facing synchronized cameras. Following the protocol in DynNeRF [65], we build the input by selecting the frames at different timestamps in a 'round-robin' manner. Then we evaluate the novel view synthesis quality at the first camera view but at different timestamps. We compare against HyperNeRF [4], DynNeRF [65], RoDynRF [33], 4D-GS [66], Casual-FVS [9] as per-scene optimization baselines.

Our results are shown in Tab. 1b and Fig. 5. Our model demonstrates performance that is competitive or exceeds that of previous optimization-based methods, ranking 3$^{\text{rd}}$ among all baselines in terms of PSNR. Compared to the explicit 3DGS-based representation [66, 9], our approach outperforms their performance by 5% on PSNR (25.82dB vs. 24.57dB). In terms of training and rendering speed, NeRF-based methods [65, 6] require multiple GPUs and/or $>$1 day for optimization. Compared to [66, 9], our feed-forward bullet-time formulation is significantly faster, requiring no optimization time and rendering in real-time.

4.2.2 Qualitative analysis

To assess the performance of our method in real-world scenarios, we select multiple monocular videos from the DAVIS dataset [67] for testing. Camera poses for the videos were estimated using

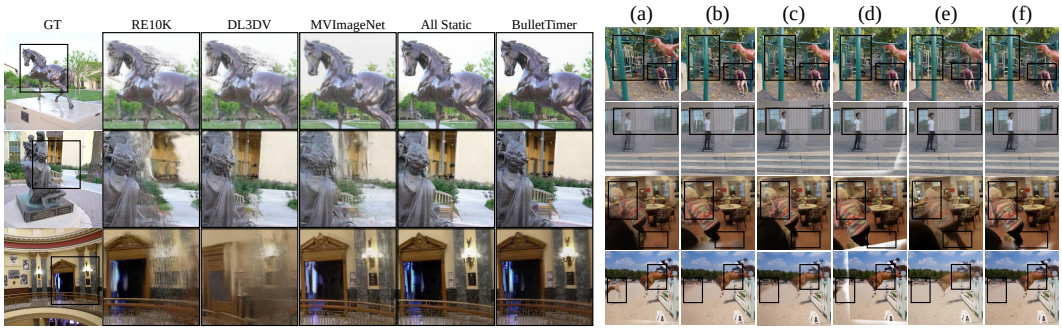

Figure 6: *Left*: **Qualitative comparison of models trained on different datasets** and evaluated on the out-of-distribution Tanks & Temples benchmark [69]. *Right*: (a) model w/o 3D Pretrain, (b) model w/ Re10K only 3D Pretrain, (c) model w/o static Co-train in **Stage 2**, (d) model w/o interpolation supervision, (e) Novel Time Enhancer model, (f) our full model. The upper two scenes are from NVIDIA dataset, and lower two scenes are from DAVIS dataset.

the same annotation technique as detailed in § 3.3. Fig. 4 shows a visualization of the results. Our model demonstrates strong generalization capabilities in real-world captures, producing high-quality, sharp renderings across a variety of objects with complex motions while maintaining robust temporal and multiview consistency.

4.3 Compatibility with static scenes

Although our model is primarily designed to handle dynamic scenes, the formulation and the training strategy enable it to be still backward compatible with static scenes. In this section, we show that the *same* model achieves competitive results on static scenes.

RealEstate10K (RE10K) benchmark [50]. We evaluate our model on the RE10K dataset and compare with several state-of-the-art models [70, 15, 14, 5]. To ensure comparability with baseline models, we train and test our model using 256×256 resolution. Fig. 7a presents a quantitative comparison on LPIPS, where our static model outperforms all the baselines. Please refer to the Supplement for more comparisons on other metrics and visualizations.

Model	LPIPS↓
GPNR [70]	0.250
PixelSplat [15]	0.142
MVSplat [14]	0.128
GS-LRM [5]	0.114
Ours-Static	0.070
Ours-Full	0.089

(a)

Model	Datasets	LPIPS↓
GS-LRM* [5]	RE10K	0.310
Ours-Static	Objaverse	0.668
	MVImageNet	0.343
	DL3DV	0.278
	All Static	0.093
Ours-Full	+Dynamic	0.093

(b)

Figure 7: **Quantitative comparisons on static datasets.** (a) results on the RE10K benchmark [50]; (b) results on the Tanks and Temples benchmark [69]. We highlight the best, second best, and third best models. *: Our reproduced results.

Tanks & Temples benchmark [69]. We further evaluate our model on an unseen test dataset, the Tanks & Temples [71] subset from the InstantSplat [69] benchmark, which consists of 10 scenes. We use the state-of-the-art novel view synthesis model [5] as our baseline, reproducing their model since the original code and weights are not publicly available. Additionally, we include our pretrained static model from **Stage 1** as an additional baseline.

To analyze the impact of our mixed-dataset pretraining strategy, we also train single-dataset models using the same training schedule as further baselines. All models utilize 4 context views. Quantitative results (Fig. 7b) demonstrate that our pretrained static model with mixed-dataset training substantially outperforms the single-dataset models, highlighting the crucial role of multi-dataset training for generalization to unseen domains. Even when incorporating the dynamic scene datasets, BTimer achieves comparable result to our best static models. § 4.2.1 provides a qualitative comparison, showing that BTimer consistently generates sharper outputs that closely align with the ground truth.

4.4 Ablation study

We study the effect of different design choices. **1) Context frames.** We visualize the reconstruction results as we progressively add 3DGS predictions from more context frames across multiple different

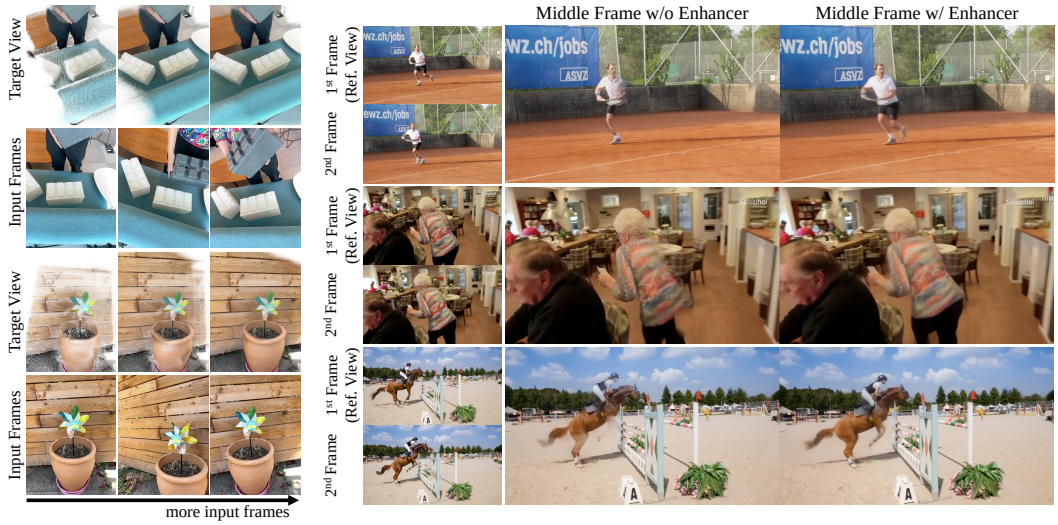

(a) (b)

Figure 8: (a) **Illustration of bullet-time reconstruction from multiple context frames.** Increased number of frame predictions leads to progressively more complete scene reconstruction on target views. (b) **Ablation on the NTE module**. The middle frame is in between the 1st frame and the 2nd frame. Results are rendered from the view of the 1st frame.

timestamps in Fig. 8a, where increasing the number of context frame leads to progressively more complete scene reconstruction. This demonstrates the flexibility of our bullet-time reconstruction formulation: during the inference stage, we can arbitrarily select spatially-distant frames that contribute to a more complete view coverage of the scene. **2) Curriculum training.** We show in § 4.2.1 the effect of our curriculum training strategy. Without **Stage 1** of pre-training on static scenes, the model struggles to produce results of correct geometry and sharp details. Pretraining on multiple diverse datasets is also crucial, which we demonstrate by *just* training on RE10K dataset, and non-negligible distortions are observed in the results. Similarly, even in **Stage 2** of our curriculum, we still need to co-train on static scenes which provide more multi-view supervisions, thus maintaining the rich details and reasonable geometries. Quantitative ablation results are shown in the Supplement. **3) Interpolation supervision.** Shown in § 4.2.1 (with more results in the Supplement), interpolation supervision (introduced in § 3.1) plays a significant role, without which the model tends to produce *white-edge* artifacts. This occurs because without interpolation loss, the model often generates 3DGS that are positioned too close to the camera with low depth values to *cheat* the loss. In contrast, adding the interpolation supervision requires the model to account for scene dynamics and encourages consistency across multiple views. **4) NTE.** As demonstrated in Fig. 8b, our NTE module enhances the bullet-time reconstruction model's ability to handle scenes with fast or complex motions, largely reducing the ghosting artifacts. Additional video results are provided in the supplementary material. Although 3D-free design enables NTE to handle complex dynamics and produce smooth transitions between adjacent frames, the model struggles to produce novel views that are far from the input camera trajectory (As illustrated in § 4.2.1).

5 Conclusion

In this paper we present BTimer, the first feed-forward dynamic 3D scene reconstruction model for novel view synthesis. We present a bullet-time formulation that allows us to train the model in a more flexible and scalable way. We demonstrate through extensive experiments that our model is able to provide high-quality results at arbitrary novel views and timestamps, outperforming the baselines in terms of both quality and efficiency.

Limitations. Our method is mainly targeted for novel view synthesis, and the recovered geometry (hence the depth map) is usually not as accurate. Correspondences between frames are implicitly modeled by the neural network, and our pixel-aligned Gaussian representation cannot represent temporal deformations. Although practically we observe temporally coherent results, additional post-processing steps have to be introduced to recover the explicit motion of the geometry.

Broader Impact. BTimer can transform posed casual videos into realistic dynamic 3D assets. However, it should be used with caution, particularly concerning privacy, copyrights, and the potential for malicious impersonation.

References

[1] Jae Shin Yoon, Kihwan Kim, Orazio Gallo, Hyun Soo Park, and Jan Kautz. Novel view synthesis of dynamic scenes with globally coherent depths from a monocular camera. In *Proceedings of the IEEE/CVF Conference on Computer Vision and Pattern Recognition*, pages 5336–5345, 2020.

[2] Zhengqi Li, Simon Niklaus, Noah Snavely, and Oliver Wang. Neural scene flow fields for space-time view synthesis of dynamic scenes. In *Proceedings of the IEEE/CVF Conference on Computer Vision and Pattern Recognition*, pages 6498–6508, 2021.

[3] Ben Mildenhall, Pratul P Srinivasan, Matthew Tancik, Jonathan T Barron, Ravi Ramamoorthi, and Ren Ng. Nerf: Representing scenes as neural radiance fields for view synthesis. *Communications of the ACM*, 65(1):99–106, 2021.

[4] Keunhong Park, Utkarsh Sinha, Peter Hedman, Jonathan T Barron, Sofien Bouaziz, Dan B Goldman, Ricardo Martin-Brualla, and Steven M Seitz. Hypernerf: A higher-dimensional representation for topologically varying neural radiance fields. *arXiv preprint arXiv:2106.13228*, 2021.

[5] Kai Zhang, Sai Bi, Hao Tan, Yuanbo Xiangli, Nanxuan Zhao, Kalyan Sunkavalli, and Zexiang Xu. Gs-lrm: Large reconstruction model for 3d gaussian splatting. In *European Conference on Computer Vision*, pages 1–19. Springer, 2025.

[6] Fengrui Tian, Shaoyi Du, and Yueqi Duan. Mononerf: Learning a generalizable dynamic radiance field from monocular videos. In *Proceedings of the IEEE/CVF International Conference on Computer Vision*, pages 17903–17913, 2023.

[7] Wenqi Xian, Jia-Bin Huang, Johannes Kopf, and Changil Kim. Space-time neural irradiance fields for free-viewpoint video. In *Proceedings of the IEEE/CVF conference on computer vision and pattern recognition*, pages 9421–9431, 2021.

[8] Zhengqi Li, Qianqian Wang, Forrester Cole, Richard Tucker, and Noah Snavely. Dynibar: Neural dynamic image-based rendering. In *Proceedings of the IEEE/CVF Conference on Computer Vision and Pattern Recognition*, pages 4273–4284, 2023.

[9] Yao-Chih Lee, Zhoutong Zhang, Kevin Blackburn-Matzen, Simon Niklaus, Jianming Zhang, Jia-Bin Huang, and Feng Liu. Fast view synthesis of casual videos with soup-of-planes. In *European Conference on Computer Vision*, pages 278–296. Springer, 2025.

[10] Qianqian Wang, Vickie Ye, Hang Gao, Jake Austin, Zhengqi Li, and Angjoo Kanazawa. Shape of motion: 4d reconstruction from a single video. *arXiv preprint arXiv:2407.13764*, 2024.

[11] Jiahui Lei, Yijia Weng, Adam Harley, Leonidas Guibas, and Kostas Daniilidis. Mosca: Dynamic gaussian fusion from casual videos via 4d motion scaffolds. *arXiv preprint arXiv:2405.17421*, 2024.

[12] Yicong Hong, Kai Zhang, Jiuxiang Gu, Sai Bi, Yang Zhou, Difan Liu, Feng Liu, Kalyan Sunkavalli, Trung Bui, and Hao Tan. Lrm: Large reconstruction model for single image to 3d. *arXiv preprint arXiv:2311.04400*, 2023.

[13] Wenyan Cong, Hanxue Liang, Peihao Wang, Zhiwen Fan, Tianlong Chen, Mukund Varma, Yi Wang, and Zhangyang Wang. Enhancing nerf akin to enhancing llms: Generalizable nerf transformer with mixture-of-view-experts. In *Proceedings of the IEEE/CVF International Conference on Computer Vision*, pages 3193–3204, 2023.

[14] Yuedong Chen, Haofei Xu, Chuanxia Zheng, Bohan Zhuang, Marc Pollefeys, Andreas Geiger, Tat-Jen Cham, and Jianfei Cai. Mvsplat: Efficient 3d gaussian splatting from sparse multi-view images. In *European Conference on Computer Vision*, pages 370–386. Springer, 2025.

[15] David Charatan, Sizhe Lester Li, Andrea Tagliasacchi, and Vincent Sitzmann. pixelsplat: 3d gaussian splats from image pairs for scalable generalizable 3d reconstruction. In *Proceedings of the IEEE/CVF Conference on Computer Vision and Pattern Recognition*, pages 19457–19467, 2024.

[16] Haian Jin, Hanwen Jiang, Hao Tan, Kai Zhang, Sai Bi, Tianyuan Zhang, Fujun Luan, Noah Snavely, and Zexiang Xu. Lvsm: A large view synthesis model with minimal 3d inductive bias. *arXiv preprint arXiv:2410.17242*, 2024.

[17] Jiawei Ren, Kevin Xie, Ashkan Mirzaei, Hanxue Liang, Xiaohui Zeng, Karsten Kreis, Ziwei Liu, Antonio Torralba, Sanja Fidler, Seung Wook Kim, et al. L4gm: Large 4d gaussian reconstruction model. *arXiv preprint arXiv:2406.10324*, 2024.

[18] Bernhard Kerbl, Georgios Kopanas, Thomas Leimkühler, and George Drettakis. 3d gaussian splatting for real-time radiance field rendering. *ACM Trans. Graph.*, 42(4):139–1, 2023.

[19] Lingjie Liu, Jiatao Gu, Kyaw Zaw Lin, Tat-Seng Chua, and Christian Theobalt. Neural sparse voxel fields. *Advances in Neural Information Processing Systems*, 33:15651–15663, 2020.

[20] Francis Williams, Jiahui Huang, Jonathan Swartz, Gergely Klar, Vijay Thakkar, Matthew Cong, Xuanchi Ren, Ruilong Li, Clement Fuji-Tsang, Sanja Fidler, Eftychios Sifakis, and Ken Museth. fvdb: A deep-learning framework for sparse, large-scale, and high-performance spatial intelligence. *ACM Transactions on Graphics (TOG)*, 43(4):133:1–133:15, 2024.

[21] Lars Mescheder, Michael Oechsle, Michael Niemeyer, Sebastian Nowozin, and Andreas Geiger. Occupancy networks: Learning 3d reconstruction in function space. In *Proceedings of the IEEE/CVF conference on computer vision and pattern recognition*, pages 4460–4470, 2019.

[22] Thomas Müller, Alex Evans, Christoph Schied, and Alexander Keller. Instant neural graphics primitives with a multiresolution hash encoding. *ACM transactions on graphics (TOG)*, 41(4):1–15, 2022.

[23] Kara-Ali Aliev, Artem Sevastopolsky, Maria Kolos, Dmitry Ulyanov, and Victor Lempitsky. Neural point-based graphics. In *Computer Vision–ECCV 2020: 16th European Conference, Glasgow, UK, August 23–28, 2020, Proceedings, Part XXII 16*, pages 696–712. Springer, 2020.

[24] Sara Fridovich-Keil, Giacomo Meanti, Frederik Rahbæk Warburg, Benjamin Recht, and Angjoo Kanazawa. K-planes: Explicit radiance fields in space, time, and appearance. In *Proceedings of the IEEE/CVF Conference on Computer Vision and Pattern Recognition*, pages 12479–12488, 2023.

[25] Ang Cao and Justin Johnson. Hexplane: A fast representation for dynamic scenes. In *Proceedings of the IEEE/CVF Conference on Computer Vision and Pattern Recognition*, pages 130–141, 2023.

[26] Zeyu Yang, Hongye Yang, Zijie Pan, and Li Zhang. Real-time photorealistic dynamic scene representation and rendering with 4d gaussian splatting. *arXiv preprint arXiv:2310.10642*, 2023.

[27] Yuanxing Duan, Fangyin Wei, Qiyu Dai, Yuhang He, Wenzheng Chen, and Baoquan Chen. 4d-rotor gaussian splatting: towards efficient novel view synthesis for dynamic scenes. In *ACM SIGGRAPH 2024 Conference Papers*, pages 1–11, 2024.

[28] Mojtaba Bemana, Karol Myszkowski, Hans-Peter Seidel, and Tobias Ritschel. X-fields: Implicit neural view-, light-and time-image interpolation. *ACM Transactions on Graphics (TOG)*, 39(6):1–15, 2020.

[29] Richard Tucker and Noah Snavely. Single-view view synthesis with multiplane images. In *Proceedings of the IEEE/CVF Conference on Computer Vision and Pattern Recognition*, pages 551–560, 2020.

[30] Albert Pumarola, Enric Corona, Gerard Pons-Moll, and Francesc Moreno-Noguer. D-nerf: Neural radiance fields for dynamic scenes. In *Proceedings of the IEEE/CVF Conference on Computer Vision and Pattern Recognition*, pages 10318–10327, 2021.

[31] Tianye Li, Mira Slavcheva, Michael Zollhoefer, Simon Green, Christoph Lassner, Changil Kim, Tanner Schmidt, Steven Lovegrove, Michael Goesele, Richard Newcombe, et al. Neural 3d video synthesis from multi-view video. In *Proceedings of the IEEE/CVF Conference on Computer Vision and Pattern Recognition*, pages 5521–5531, 2022.

[32] Keunhong Park, Utkarsh Sinha, Jonathan T Barron, Sofien Bouaziz, Dan B Goldman, Steven M Seitz, and Ricardo Martin-Brualla. Nerfies: Deformable neural radiance fields. In *Proceedings of the IEEE/CVF International Conference on Computer Vision*, pages 5865–5874, 2021.

[33] Yu-Lun Liu, Chen Gao, Andreas Meuleman, Hung-Yu Tseng, Ayush Saraf, Changil Kim, Yung-Yu Chuang, Johannes Kopf, and Jia-Bin Huang. Robust dynamic radiance fields. In *Proceedings of the IEEE/CVF Conference on Computer Vision and Pattern Recognition*, pages 13–23, 2023.

[34] Benjamin Attal, Jia-Bin Huang, Christian Richardt, Michael Zollhoefer, Johannes Kopf, Matthew O'Toole, and Changil Kim. Hyperreel: High-fidelity 6-dof video with ray-conditioned sampling. In *Proceedings of the IEEE/CVF Conference on Computer Vision and Pattern Recognition*, pages 16610–16620, 2023.

[35] Yao-Chih Lee, Zhoutong Zhang, and Kevin Blackburn-Matzen. Fast view synthesis of casual videos with soup-of-planes. 2023.

[36] Shizun Wang, Xingyi Yang, Qiuhong Shen, Zhenxiang Jiang, and Xinchao Wang. Gflow: Recovering 4d world from monocular video. *arXiv preprint arXiv:2405.18426*, 2024.

[37] Peihao Wang, Xuxi Chen, Tianlong Chen, Subhashini Venugopalan, Zhangyang Wang, et al. Is attention all that nerf needs? *arXiv preprint arXiv:2207.13298*, 2022.

[38] Xuanchi Ren, Yifan Lu, Hanxue Liang, Zhangjie Wu, Huan Ling, Mike Chen, Sanja Fidler, Francis Williams, and Jiahui Huang. Scube: Instant large-scale scene reconstruction using voxsplats. *arXiv preprint arXiv:2410.20030*, 2024.

[39] Xiaoming Zhao, R Alex Colburn, Fangchang Ma, Miguel Ángel Bautista, Joshua M Susskind, and Alex Schwing. Pseudo-generalized dynamic view synthesis from a video. In *The Twelfth International Conference on Learning Representations*, 2024.

[40] Junyi Zhang, Charles Herrmann, Junhwa Hur, Varun Jampani, Trevor Darrell, Forrester Cole, Deqing Sun, and Ming-Hsuan Yang. Monst3r: A simple approach for estimating geometry in the presence of motion. *arXiv preprint arXiv:2410.03825*, 2024.

[41] Alexey Dosovitskiy. An image is worth 16x16 words: Transformers for image recognition at scale. *arXiv preprint arXiv:2010.11929*, 2020.

[42] Jimmy Lei Ba. Layer normalization. *arXiv preprint arXiv:1607.06450*, 2016.

[43] Yinghao Xu, Hao Tan, Fujun Luan, Sai Bi, Peng Wang, Jiahao Li, Zifan Shi, Kalyan Sunkavalli, Gordon Wetzstein, Zexiang Xu, et al. Dmv3d: Denoising multi-view diffusion using 3d large reconstruction model. *arXiv preprint arXiv:2311.09217*, 2023.

[44] A Vaswani. Attention is all you need. *Advances in Neural Information Processing Systems*, 2017.

[45] Richard Zhang, Phillip Isola, Alexei A Efros, Eli Shechtman, and Oliver Wang. The unreasonable effectiveness of deep features as a perceptual metric. In *CVPR*, 2018.

[46] Reiner Pope, Sholto Douglas, Aakanksha Chowdhery, Jacob Devlin, James Bradbury, Jonathan Heek, Kefan Xiao, Shivani Agrawal, and Jeff Dean. Efficiently scaling transformer inference. *Proceedings of Machine Learning and Systems*, 5:606–624, 2023.

[47] Richard Sutton. The bitter lesson. *Incomplete Ideas (blog)*, 13(1):38, 2019.

[48] Josh Achiam, Steven Adler, Sandhini Agarwal, Lama Ahmad, Ilge Akkaya, Florencia Leoni Aleman, Diogo Almeida, Janko Altenschmidt, Sam Altman, Shyamal Anadkat, et al. Gpt-4 technical report. *arXiv preprint arXiv:2303.08774*, 2023.

[49] Matt Deitke, Dustin Schwenk, Jordi Salvador, Luca Weihs, Oscar Michel, Eli VanderBilt, Ludwig Schmidt, Kiana Ehsani, Aniruddha Kembhavi, and Ali Farhadi. Objaverse: A universe of annotated 3d objects. In *Proceedings of the IEEE/CVF Conference on Computer Vision and Pattern Recognition*, pages 13142–13153, 2023.

[50] Tinghui Zhou, Richard Tucker, John Flynn, Graham Fyffe, and Noah Snavely. Stereo magnification: Learning view synthesis using multiplane images. *arXiv preprint arXiv:1805.09817*, 2018.

[51] Xianggang Yu, Mutian Xu, Yidan Zhang, Haolin Liu, Chongjie Ye, Yushuang Wu, Zizheng Yan, Chenming Zhu, Zhangyang Xiong, Tianyou Liang, et al. Mvimgnet: A large-scale dataset of multi-view images. In *Proceedings of the IEEE/CVF conference on computer vision and pattern recognition*, pages 9150–9161, 2023.

[52] Lu Ling, Yichen Sheng, Zhi Tu, Wentian Zhao, Cheng Xin, Kun Wan, Lantao Yu, Qianyu Guo, Zixun Yu, Yawen Lu, et al. Dl3dv-10k: A large-scale scene dataset for deep learning-based 3d vision. In *Proceedings of the IEEE/CVF Conference on Computer Vision and Pattern Recognition*, pages 22160–22169, 2024.

[53] Klaus Greff, Francois Belletti, Lucas Beyer, Carl Doersch, Yilun Du, Daniel Duckworth, David J Fleet, Dan Gnanapragasam, Florian Golemo, Charles Herrmann, et al. Kubric: A scalable dataset generator. In *Proceedings of the IEEE/CVF conference on computer vision and pattern recognition*, pages 3749–3761, 2022.

[54] Yang Zheng, Adam W. Harley, Bokui Shen, Gordon Wetzstein, and Leonidas J. Guibas. Pointodyssey: A large-scale synthetic dataset for long-term point tracking. In *ICCV*, 2023.

[55] Nikita Karaev, Ignacio Rocco, Benjamin Graham, Natalia Neverova, Andrea Vedaldi, and Christian Rupprecht. Dynamicstereo: Consistent dynamic depth from stereo videos. *CVPR*, 2023.

[56] Lukas Mehl, Jenny Schmalfuss, Azin Jahedi, Yaroslava Nalivayko, and Andrés Bruhn. Spring: A high-resolution high-detail dataset and benchmark for scene flow, optical flow and stereo. In *Proceedings of the IEEE/CVF Conference on Computer Vision and Pattern Recognition*, pages 4981–4991, 2023.

[57] Tsai-Shien Chen, Aliaksandr Siarohin, Willi Menapace, Ekaterina Deyneka, Hsiang-wei Chao, Byung Eun Jeon, Yuwei Fang, Hsin-Ying Lee, Jian Ren, Ming-Hsuan Yang, et al. Panda-70m: Captioning 70m videos with multiple cross-modality teachers. In *Proceedings of the IEEE/CVF Conference on Computer Vision and Pattern Recognition*, pages 13320–13331, 2024.

[58] Alexander Kirillov, Eric Mintun, Nikhila Ravi, Hanzi Mao, Chloe Rolland, Laura Gustafson, Tete Xiao, Spencer Whitehead, Alexander C Berg, Wan-Yen Lo, et al. Segment anything. In *Proceedings of the IEEE/CVF International Conference on Computer Vision*, pages 4015–4026, 2023.

[59] Zachary Teed and Jia Deng. Droid-slam: Deep visual slam for monocular, stereo, and rgb-d cameras. *Advances in neural information processing systems*, 34:16558–16569, 2021.

[60] Tri Dao. Flashattention-2: Faster attention with better parallelism and work partitioning. *arXiv preprint arXiv:2307.08691*, 2023.

[61] Horace He, Driss Guessous, Yanbo Liang, and Joy Dong. FlexAttention: The Flexibility of PyTorch with the Performance of FlashAttention. `https://pytorch.org/blog/flexattention/`, August 2024.

[62] Vickie Ye, Ruilong Li, Justin Kerr, Matias Turkulainen, Brent Yi, Zhuoyang Pan, Otto Seiskari, Jianbo Ye, Jeffrey Hu, Matthew Tancik, and Angjoo Kanazawa. gsplat: An open-source library for Gaussian splatting. *arXiv preprint arXiv:2409.06765*, 2024.

[63] Jiemin Fang, Taoran Yi, Xinggang Wang, Lingxi Xie, Xiaopeng Zhang, Wenyu Liu, Matthias Nießner, and Qi Tian. Fast dynamic radiance fields with time-aware neural voxels. In *SIGGRAPH Asia 2022 Conference Papers*, pages 1–9, 2022.

[64] Hang Gao, Ruilong Li, Shubham Tulsiani, Bryan Russell, and Angjoo Kanazawa. Monocular dynamic view synthesis: A reality check. *Advances in Neural Information Processing Systems*, 35:33768–33780, 2022.

[65] Chen Gao, Ayush Saraf, Johannes Kopf, and Jia-Bin Huang. Dynamic view synthesis from dynamic monocular video. In *Proceedings of the IEEE/CVF International Conference on Computer Vision*, pages 5712–5721, 2021.

[66] Guanjun Wu, Taoran Yi, Jiemin Fang, Lingxi Xie, Xiaopeng Zhang, Wei Wei, Wenyu Liu, Qi Tian, and Xinggang Wang. 4d gaussian splatting for real-time dynamic scene rendering. In *Proceedings of the IEEE/CVF Conference on Computer Vision and Pattern Recognition*, pages 20310–20320, 2024.

[67] Federico Perazzi, Jordi Pont-Tuset, Brian McWilliams, Luc Van Gool, Markus Gross, and Alexander Sorkine-Hornung. A benchmark dataset and evaluation methodology for video object segmentation. In *Proceedings of the IEEE conference on computer vision and pattern recognition*, pages 724–732, 2016.

[68] Zhou Wang, Alan C Bovik, Hamid R Sheikh, and Eero P Simoncelli. Image quality assessment: from error visibility to structural similarity. *IEEE transactions on image processing*, 13(4):600–612, 2004.

[69] Zhiwen Fan, Wenyan Cong, Kairun Wen, Kevin Wang, Jian Zhang, Xinghao Ding, Danfei Xu, Boris Ivanovic, Marco Pavone, Georgios Pavlakos, et al. Instantsplat: Unbounded sparse-view pose-free gaussian splatting in 40 seconds. *arXiv preprint arXiv:2403.20309*, 2, 2024.

[70] Mohammed Suhail, Carlos Esteves, Leonid Sigal, and Ameesh Makadia. Generalizable patch-based neural rendering. In *European Conference on Computer Vision*, pages 156–174. Springer, 2022.

[71] Arno Knapitsch, Jaesik Park, Qian-Yi Zhou, and Vladlen Koltun. Tanks and temples: Benchmarking large-scale scene reconstruction. *ACM Transactions on Graphics (ToG)*, 36(4):1–13, 2017.

[72] Jiaxiang Tang, Zhaoxi Chen, Xiaokang Chen, Tengfei Wang, Gang Zeng, and Ziwei Liu. Lgm: Large multi-view gaussian model for high-resolution 3d content creation. In *European Conference on Computer Vision*, pages 1–18. Springer, 2025.

[73] Alex Yu, Vickie Ye, Matthew Tancik, and Angjoo Kanazawa. pixelnerf: Neural radiance fields from one or few images. In *Proceedings of the IEEE/CVF conference on computer vision and pattern recognition*, pages 4578–4587, 2021.

[74] Yilun Du, Cameron Smith, Ayush Tewari, and Vincent Sitzmann. Learning to render novel views from wide-baseline stereo pairs. In *Proceedings of the IEEE/CVF Conference on Computer Vision and Pattern Recognition*, pages 4970–4980, 2023.

[75] Haofei Xu, Anpei Chen, Yuedong Chen, Christos Sakaridis, Yulun Zhang, Marc Pollefeys, Andreas Geiger, and Fisher Yu. Murf: Multi-baseline radiance fields. In *Proceedings of the IEEE/CVF Conference on Computer Vision and Pattern Recognition*, pages 20041–20050, 2024.

[76] Colton Stearns, Adam Harley, Mikaela Uy, Florian Dubost, Federico Tombari, Gordon Wetzstein, and Leonidas Guibas. Dynamic gaussian marbles for novel view synthesis of casual monocular videos. In *SIGGRAPH Asia 2024 Conference Papers*, pages 1–11, 2024.

[77] Minh-Quan Viet Bui, Jongmin Park, Jihyong Oh, and Munchurl Kim. Dyblurf: Dynamic deblurring neural radiance fields for blurry monocular video. *arXiv preprint arXiv:2312.13528*, 2023.

[78] Moritz Kappel, Florian Hahlbohm, Timon Scholz, Susana Castillo, Christian Theobalt, Martin Eisemann, Vladislav Golyanik, and Marcus Magnor. D-npc: Dynamic neural point clouds for non-rigid view synthesis from monocular video. In *Computer Graphics Forum*, page e70038. Wiley Online Library, 2025.

[79] Jiahui Lei, Yijia Weng, Adam W Harley, Leonidas Guibas, and Kostas Daniilidis. Mosca: Dynamic gaussian fusion from casual videos via 4d motion scaffolds. In *Proceedings of the Computer Vision and Pattern Recognition Conference*, pages 6165–6177, 2025.

[80] Edgar Tretschk, Ayush Tewari, Vladislav Golyanik, Michael Zollhöfer, Christoph Lassner, and Christian Theobalt. Non-rigid neural radiance fields: Reconstruction and novel view synthesis of a dynamic scene from monocular video. In *Proceedings of the IEEE/CVF international conference on computer vision*, pages 12959–12970, 2021.

[81] Kaichen Zhou, Jia-Xing Zhong, Sangyun Shin, Kai Lu, Yiyuan Yang, Andrew Markham, and Niki Trigoni. Dynpoint: Dynamic neural point for view synthesis. *Advances in Neural Information Processing Systems*, 36:69532–69545, 2023.

[82] Yi-Hua Huang, Yang-Tian Sun, Ziyi Yang, Xiaoyang Lyu, Yan-Pei Cao, and Xiaojuan Qi. Sc-gs: Sparse-controlled gaussian splatting for editable dynamic scenes. In *Proceedings of the IEEE/CVF Conference on Computer Vision and Pattern Recognition*, pages 4220–4230, 2024.

[83] Ziqi Huang, Yinan He, Jiashuo Yu, Fan Zhang, Chenyang Si, Yuming Jiang, Yuanhan Zhang, Tianxing Wu, Qingyang Jin, Nattapol Chanpaisit, et al. Vbench: Comprehensive benchmark suite for video generative models. In *Proceedings of the IEEE/CVF Conference on Computer Vision and Pattern Recognition*, pages 21807–21818, 2024.

NeurIPS Paper Checklist

1. **Claims**

   Question: Do the main claims made in the abstract and introduction accurately reflect the paper's contributions and scope?

   Answer: [Yes]

   Justification: The claims in the abstract and introduction (§ 1) accurately reflect the paper's core contributions, including the introduction of BTimer, the first real-time feed-forward bullet-time reconstruction model for dynamic scenes. The text clearly outlines the bullet-time formulation, Novel Time Enhancer module, and curriculum training strategy, and these are consistently supported by results in § 4.

   Guidelines:

   - The answer NA means that the abstract and introduction do not include the claims made in the paper.
   - The abstract and/or introduction should clearly state the claims made, including the contributions made in the paper and important assumptions and limitations. A No or NA answer to this question will not be perceived well by the reviewers.
   - The claims made should match theoretical and experimental results, and reflect how much the results can be expected to generalize to other settings.
   - It is fine to include aspirational goals as motivation as long as it is clear that these goals are not attained by the paper.

2. **Limitations**

   Question: Does the paper discuss the limitations of the work performed by the authors?

   Answer: [Yes]

   Justification: Limitations are explicitly discussed in § 5. The paper acknowledges that while BTimer excels at novel view synthesis, the recovered geometry may lack accuracy due to the pixel-aligned 3D Gaussian formulation. It also notes that temporal deformations are not explicitly modeled and that additional post-processing may be needed for extracting motion. Ethical concerns, such as privacy and potential misuse, are also briefly mentioned.

   Guidelines:

   - The answer NA means that the paper has no limitation while the answer No means that the paper has limitations, but those are not discussed in the paper.
   - The authors are encouraged to create a separate "Limitations" section in their paper.
   - The paper should point out any strong assumptions and how robust the results are to violations of these assumptions (e.g., independence assumptions, noiseless settings, model well-specification, asymptotic approximations only holding locally). The authors should reflect on how these assumptions might be violated in practice and what the implications would be.
   - The authors should reflect on the scope of the claims made, e.g., if the approach was only tested on a few datasets or with a few runs. In general, empirical results often depend on implicit assumptions, which should be articulated.
   - The authors should reflect on the factors that influence the performance of the approach. For example, a facial recognition algorithm may perform poorly when image resolution is low or images are taken in low lighting. Or a speech-to-text system might not be used reliably to provide closed captions for online lectures because it fails to handle technical jargon.
   - The authors should discuss the computational efficiency of the proposed algorithms and how they scale with dataset size.
   - If applicable, the authors should discuss possible limitations of their approach to address problems of privacy and fairness.
   - While the authors might fear that complete honesty about limitations might be used by reviewers as grounds for rejection, a worse outcome might be that reviewers discover limitations that aren't acknowledged in the paper. The authors should use their best

judgment and recognize that individual actions in favor of transparency play an important role in developing norms that preserve the integrity of the community. Reviewers will be specifically instructed to not penalize honesty concerning limitations.

3. **Theory assumptions and proofs**

   Question: For each theoretical result, does the paper provide the full set of assumptions and a complete (and correct) proof?

   Answer: [NA]

   Justification: The paper does not include theoretical results.

   Guidelines:

   - The answer NA means that the paper does not include theoretical results.
   - All the theorems, formulas, and proofs in the paper should be numbered and cross-referenced.
   - All assumptions should be clearly stated or referenced in the statement of any theorems.
   - The proofs can either appear in the main paper or the supplemental material, but if they appear in the supplemental material, the authors are encouraged to provide a short proof sketch to provide intuition.
   - Inversely, any informal proof provided in the core of the paper should be complemented by formal proofs provided in appendix or supplemental material.
   - Theorems and Lemmas that the proof relies upon should be properly referenced.

4. **Experimental result reproducibility**

   Question: Does the paper fully disclose all the information needed to reproduce the main experimental results of the paper to the extent that it affects the main claims and/or conclusions of the paper (regardless of whether the code and data are provided or not)?

   Answer: [Yes]

   Justification: § 4.1 provides detailed training and inference settings, including hardware setup, training stages and schedules, learning rates, architecture details (e.g., ViT backbone with FlashAttention-3), and data sources. Although code is not yet released, the described information is sufficient to reproduce key results.

   Guidelines:

   - The answer NA means that the paper does not include experiments.
   - If the paper includes experiments, a No answer to this question will not be perceived well by the reviewers: Making the paper reproducible is important, regardless of whether the code and data are provided or not.
   - If the contribution is a dataset and/or model, the authors should describe the steps taken to make their results reproducible or verifiable.
   - Depending on the contribution, reproducibility can be accomplished in various ways. For example, if the contribution is a novel architecture, describing the architecture fully might suffice, or if the contribution is a specific model and empirical evaluation, it may be necessary to either make it possible for others to replicate the model with the same dataset, or provide access to the model. In general. releasing code and data is often one good way to accomplish this, but reproducibility can also be provided via detailed instructions for how to replicate the results, access to a hosted model (e.g., in the case of a large language model), releasing of a model checkpoint, or other means that are appropriate to the research performed.
   - While NeurIPS does not require releasing code, the conference does require all submissions to provide some reasonable avenue for reproducibility, which may depend on the nature of the contribution. For example
     (a) If the contribution is primarily a new algorithm, the paper should make it clear how to reproduce that algorithm.
     (b) If the contribution is primarily a new model architecture, the paper should describe the architecture clearly and fully.

(c) If the contribution is a new model (e.g., a large language model), then there should either be a way to access this model for reproducing the results or a way to reproduce the model (e.g., with an open-source dataset or instructions for how to construct the dataset).

(d) We recognize that reproducibility may be tricky in some cases, in which case authors are welcome to describe the particular way they provide for reproducibility. In the case of closed-source models, it may be that access to the model is limited in some way (e.g., to registered users), but it should be possible for other researchers to have some path to reproducing or verifying the results.

5. **Open access to data and code**

   Question: Does the paper provide open access to the data and code, with sufficient instructions to faithfully reproduce the main experimental results, as described in supplemental material?

   Answer: [No]

   Justification: Due to institutional constraints, we are not able to release the code until it is fully reviewed by the legal team. We do not have an ETA for this process. We will update the paper with a link to the code as soon as it is available.

   Guidelines:

   - The answer NA means that paper does not include experiments requiring code.
   - Please see the NeurIPS code and data submission guidelines (`https://nips.cc/public/guides/CodeSubmissionPolicy`) for more details.
   - While we encourage the release of code and data, we understand that this might not be possible, so "No" is an acceptable answer. Papers cannot be rejected simply for not including code, unless this is central to the contribution (e.g., for a new open-source benchmark).
   - The instructions should contain the exact command and environment needed to run to reproduce the results. See the NeurIPS code and data submission guidelines (`https://nips.cc/public/guides/CodeSubmissionPolicy`) for more details.
   - The authors should provide instructions on data access and preparation, including how to access the raw data, preprocessed data, intermediate data, and generated data, etc.
   - The authors should provide scripts to reproduce all experimental results for the new proposed method and baselines. If only a subset of experiments are reproducible, they should state which ones are omitted from the script and why.
   - At submission time, to preserve anonymity, the authors should release anonymized versions (if applicable).
   - Providing as much information as possible in supplemental material (appended to the paper) is recommended, but including URLs to data and code is permitted.

6. **Experimental setting/details**

   Question: Does the paper specify all the training and test details (e.g., data splits, hyperparameters, how they were chosen, type of optimizer, etc.) necessary to understand the results?

   Answer:[Yes]

   Justification: § 4.1 thoroughly describes training stages, dataset splits, hyperparameters, learning rate schedules, optimizer configurations, and model scaling. It also details how real-world videos are processed. The ablations in § 4.4 complement this by clarifying the effect of each design choice.

   Guidelines:

   - The answer NA means that the paper does not include experiments.
   - The experimental setting should be presented in the core of the paper to a level of detail that is necessary to appreciate the results and make sense of them.
   - The full details can be provided either with the code, in appendix, or as supplemental material.

7. **Experiment statistical significance**

Question: Does the paper report error bars suitably and correctly defined or other appropriate information about the statistical significance of the experiments?

Answer: [No]

Justification: Due to the high computational cost of training large models over multiple GPUs and datasets, statistical significance tests (e.g., error bars) are not provided. However, ablation studies and comparisons across multiple datasets offer strong empirical support for the claims.

Guidelines:

- The answer NA means that the paper does not include experiments.
- The authors should answer "Yes" if the results are accompanied by error bars, confidence intervals, or statistical significance tests, at least for the experiments that support the main claims of the paper.
- The factors of variability that the error bars are capturing should be clearly stated (for example, train/test split, initialization, random drawing of some parameter, or overall run with given experimental conditions).
- The method for calculating the error bars should be explained (closed form formula, call to a library function, bootstrap, etc.)
- The assumptions made should be given (e.g., Normally distributed errors).
- It should be clear whether the error bar is the standard deviation or the standard error of the mean.
- It is OK to report 1-sigma error bars, but one should state it. The authors should preferably report a 2-sigma error bar than state that they have a 96% CI, if the hypothesis of Normality of errors is not verified.
- For asymmetric distributions, the authors should be careful not to show in tables or figures symmetric error bars that would yield results that are out of range (e.g. negative error rates).
- If error bars are reported in tables or plots, The authors should explain in the text how they were calculated and reference the corresponding figures or tables in the text.

8. **Experiments compute resources**

   Question: For each experiment, does the paper provide sufficient information on the computer resources (type of compute workers, memory, time of execution) needed to reproduce the experiments?

   Answer: [Yes]

   Justification: Please refer to § 4.1 for more details on compute resources.

   Guidelines:

   - The answer NA means that the paper does not include experiments.
   - The paper should indicate the type of compute workers CPU or GPU, internal cluster, or cloud provider, including relevant memory and storage.
   - The paper should provide the amount of compute required for each of the individual experimental runs as well as estimate the total compute.
   - The paper should disclose whether the full research project required more compute than the experiments reported in the paper (e.g., preliminary or failed experiments that didn't make it into the paper).

9. **Code of ethics**

   Question: Does the research conducted in the paper conform, in every respect, with the NeurIPS Code of Ethics `https://neurips.cc/public/EthicsGuidelines`?

   Answer: [Yes]

   Justification: The research conducted in the paper conform, in every respect, with the NeurIPS Code of Ethics.

   Guidelines:

   - The answer NA means that the authors have not reviewed the NeurIPS Code of Ethics.

- If the authors answer No, they should explain the special circumstances that require a deviation from the Code of Ethics.
- The authors should make sure to preserve anonymity (e.g., if there is a special consideration due to laws or regulations in their jurisdiction).

10. **Broader impacts**

    Question: Does the paper discuss both potential positive societal impacts and negative societal impacts of the work performed?

    Answer: [Yes]

    Justification: We have provided relevant discussions in § 5.

    Guidelines:

    - The answer NA means that there is no societal impact of the work performed.
    - If the authors answer NA or No, they should explain why their work has no societal impact or why the paper does not address societal impact.
    - Examples of negative societal impacts include potential malicious or unintended uses (e.g., disinformation, generating fake profiles, surveillance), fairness considerations (e.g., deployment of technologies that could make decisions that unfairly impact specific groups), privacy considerations, and security considerations.
    - The conference expects that many papers will be foundational research and not tied to particular applications, let alone deployments. However, if there is a direct path to any negative applications, the authors should point it out. For example, it is legitimate to point out that an improvement in the quality of generative models could be used to generate deepfakes for disinformation. On the other hand, it is not needed to point out that a generic algorithm for optimizing neural networks could enable people to train models that generate Deepfakes faster.
    - The authors should consider possible harms that could arise when the technology is being used as intended and functioning correctly, harms that could arise when the technology is being used as intended but gives incorrect results, and harms following from (intentional or unintentional) misuse of the technology.
    - If there are negative societal impacts, the authors could also discuss possible mitigation strategies (e.g., gated release of models, providing defenses in addition to attacks, mechanisms for monitoring misuse, mechanisms to monitor how a system learns from feedback over time, improving the efficiency and accessibility of ML).

11. **Safeguards**

    Question: Does the paper describe safeguards that have been put in place for responsible release of data or models that have a high risk for misuse (e.g., pretrained language models, image generators, or scraped datasets)?

    Answer: [NA]

    Justification: The paper poses no such risks.

    Guidelines:

    - The answer NA means that the paper poses no such risks.
    - Released models that have a high risk for misuse or dual-use should be released with necessary safeguards to allow for controlled use of the model, for example by requiring that users adhere to usage guidelines or restrictions to access the model or implementing safety filters.
    - Datasets that have been scraped from the Internet could pose safety risks. The authors should describe how they avoided releasing unsafe images.
    - We recognize that providing effective safeguards is challenging, and many papers do not require this, but we encourage authors to take this into account and make a best faith effort.

12. **Licenses for existing assets**

    Question: Are the creators or original owners of assets (e.g., code, data, models), used in the paper, properly credited and are the license and terms of use explicitly mentioned and properly respected?

Answer: [Yes]

Justification: The paper uses several publicly available datasets and tools (e.g., Objaverse, RE10K, PANDA-70M, DROID-SLAM, FlashAttention, gsplat), all of which are cited appropriately. The terms of use and licenses are respected, as discussed in § 4.1.

Guidelines:

- The answer NA means that the paper does not use existing assets.
- The authors should cite the original paper that produced the code package or dataset.
- The authors should state which version of the asset is used and, if possible, include a URL.
- The name of the license (e.g., CC-BY 4.0) should be included for each asset.
- For scraped data from a particular source (e.g., website), the copyright and terms of service of that source should be provided.
- If assets are released, the license, copyright information, and terms of use in the package should be provided. For popular datasets, `paperswithcode.com/datasets` has curated licenses for some datasets. Their licensing guide can help determine the license of a dataset.
- For existing datasets that are re-packaged, both the original license and the license of the derived asset (if it has changed) should be provided.
- If this information is not available online, the authors are encouraged to reach out to the asset's creators.

13. **New assets**

Question: Are new assets introduced in the paper well documented and is the documentation provided alongside the assets?

Answer: [NA]

Justification: The paper does not release new assets.

Guidelines:

- The answer NA means that the paper does not release new assets.
- Researchers should communicate the details of the dataset/code/model as part of their submissions via structured templates. This includes details about training, license, limitations, etc.
- The paper should discuss whether and how consent was obtained from people whose asset is used.
- At submission time, remember to anonymize your assets (if applicable). You can either create an anonymized URL or include an anonymized zip file.

14. **Crowdsourcing and research with human subjects**

Question: For crowdsourcing experiments and research with human subjects, does the paper include the full text of instructions given to participants and screenshots, if applicable, as well as details about compensation (if any)?

Answer: [NA]

Justification: The work does not include experiments nor research with human subjects.

Guidelines:

- The answer NA means that the paper does not involve crowdsourcing nor research with human subjects.
- Including this information in the supplemental material is fine, but if the main contribution of the paper involves human subjects, then as much detail as possible should be included in the main paper.
- According to the NeurIPS Code of Ethics, workers involved in data collection, curation, or other labor should be paid at least the minimum wage in the country of the data collector.

15. **Institutional review board (IRB) approvals or equivalent for research with human subjects**

Question: Does the paper describe potential risks incurred by study participants, whether such risks were disclosed to the subjects, and whether Institutional Review Board (IRB) approvals (or an equivalent approval/review based on the requirements of your country or institution) were obtained?

Answer: [NA]

Justification: No experiments involving human subjects were conducted, and no IRB process is applicable to the methodology or data used.

Guidelines:

- The answer NA means that the paper does not involve crowdsourcing nor research with human subjects.
- Depending on the country in which research is conducted, IRB approval (or equivalent) may be required for any human subjects research. If you obtained IRB approval, you should clearly state this in the paper.
- We recognize that the procedures for this may vary significantly between institutions and locations, and we expect authors to adhere to the NeurIPS Code of Ethics and the guidelines for their institution.
- For initial submissions, do not include any information that would break anonymity (if applicable), such as the institution conducting the review.

16. **Declaration of LLM usage**

Question: Does the paper describe the usage of LLMs if it is an important, original, or non-standard component of the core methods in this research? Note that if the LLM is used only for writing, editing, or formatting purposes and does not impact the core methodology, scientific rigorousness, or originality of the research, declaration is not required.

Answer: [NA]

Justification: The paper does not include usage of LLMs.

Guidelines:

- The answer NA means that the core method development in this research does not involve LLMs as any important, original, or non-standard components.
- Please refer to our LLM policy (`https://neurips.cc/Conferences/2025/LLM`) for what should or should not be described.

Supplementary Material

In this supplementary material, we provide additional details on the datasets used in our experiments (§ F) and our training cost and more ablation studies (§ G). On the results side, we first show more qualitative static and dynamic reconstruction results (§ H, § I). We further justify our choice of the bullet-time formulation by showing that our reconstruction is **temporally smooth** (§ J), as well as an simple extension to unlock the power for **estimating dynamic deformations** (§ K).

F Dataset Details

The static datasets used in our training are as follows: OBJAVERSE [49] is a synthetic object-centric dataset, and we use the 80K-object subset from [72]. MVIMGNET [51] is a real-world object-centric dataset that has 220K objects. RE10K [50] is a real-world scene dataset that has 80K video clips. DL3DV [52] is a real-world scene dataset that has 10K video. We sample DL3DV 10 times more frequently than other datasets to balance the number of training samples. We use a spatial scale of 8 for Objaverse and scale 1 for all other datasets.

The dynamic datasets used in our training are as follows: KUBRICMV is a synthetic multi-vew video dataset that has 3K scenes. We rendered this dataset using the Kubric [53] engine. The scene setup follows Movi-E [53] and videos are rendered from all camera poses in the camera trajectory so it produces a multi-view video. POINTODYSSEY [54] is a synthetic monocular dataset with 131 scenes. DYNAMICREPLICA [55] is a synthetic stereo video dataset with 484 training sequences. SPRING [56] is a synthetic stereo video dataset with 37 scenes. PANDA-70M [57] is a real-world monocular video dataset. We use around 40K clips filtered from a random subset. We use scale 6 for Spring and DynamicReplica and 1 for other datasets. More details can be found in Tab. S2

Dataset	Dynamic	Subject	Domain	#Views	#Frames	#Scenes	#Multiplies	#Scale
RE10K [50]		*S*	Real	-	10M	80K	1	1
MVImgNet [51]		*O*	Real	-	6.5M	220K	1	1
Objaverse [49]		*O*	Synthetic	-	4M	80K	1	8
DL3DV [52]		*S*	Real	-	51M	10K	10	1
PointOdyssey [54]	✓	*O+S*	Synthetic	1	6K	131	3e3	1
Kubric-MV [53]	✓	*O+S*	Synthetic	24	70K	3K	2e2	1
DynamicReplica [55]	✓	*O+S*	Synthetic	2	145K	484	8e2	6
Spring [56]	✓	*O+S*	Synthetic	2	200K	37	1e4	6
PANDA-70M [57]	✓	*O+S*	Real	1	19M	40K	10	1

Table S2: **Datasets. Dynamic** indicates if the dataset is dynamic or static. **Subject** indicates if the dataset is object-centric (*O*) or scene-centric (*S*). **Domain** indicates if the dataset is captured from the real world or is synthesized. **#Views** denotes the number of synchronized views for a dynamic video. **#Frames** and **#Scenes** are the numbers of image frames and unique scenes in the dataset respectively. **#Multiplies** denotes the number of multiplies we sample the dataset (by scene) in training for balance. **#Scale** is the scale we applied to the dataset so that all datasets have approximately the same metric scale.

G Training Cost Analysis and Effect of Batch Size

The full training of BulletTimer takes $\sim$4 days on 32 NVIDIA A100 GPUs. As illustrated in Fig. S9, the training cost is comparable to existing feed-forward 3D reconstruction methods, such as LVSM [16] and LRM [12] (384 GPU-days) or GS-LRM [5] (192 GPU-days). Like these methods, our work also functions as an amortized algorithm: once trained, the inference cost becomes negligible. Taking inference cost also into consideration, per-scene optimization quickly becomes more expensive, with the difference becoming more pronounced with the growing number of scenes.

Fig. S10 shows the results of training our model with 1 GPU, 8 GPUs, and 32 GPUs. Although inference fits on a single GPU, our training benefits from large batch sizes so we used 32 GPUs (each

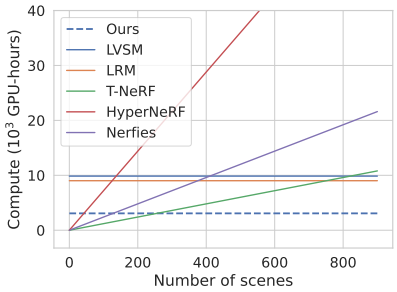

Figure S9: Computation cost.

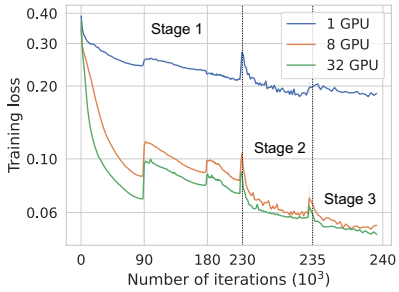

Figure S10: Batch-size ablation.

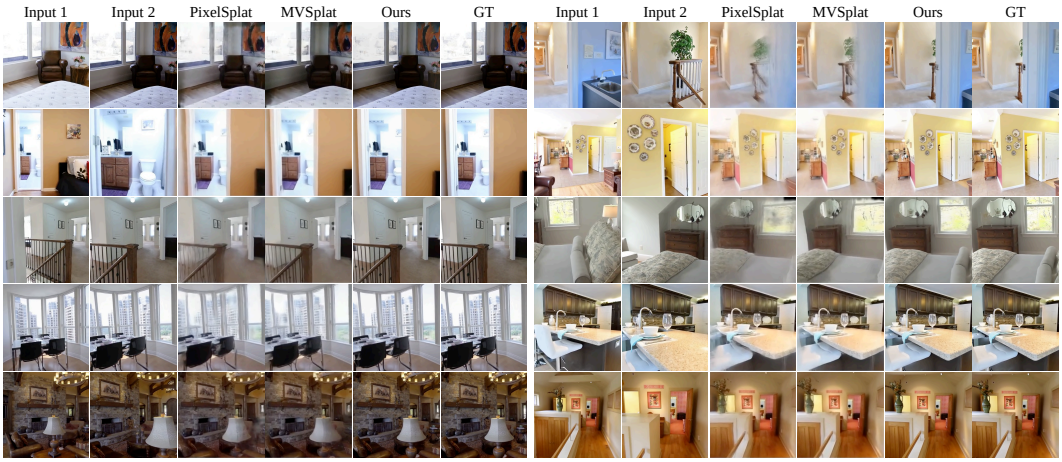

Figure S11: **Comparison on static scene dataset.** We compare our renderings with the baseline models, trained and tested on the RE10K dataset.

GPU holds a single batch). The same number of GPUs was also used in both LVSM and GS-LRM. In line with other fields (LLMs, GenAI), we regard the scalability of our method one of its key strengths. For ease of reproduction and fine-tuning, we will release our source code and pretrained checkpoints. To provide a more rigorous assessment of runtime, we have conducted an additional study varying both the number of context frames and the input resolution (see Tab. S8). The results show that BTimer consistently remains in the second range (even at 512×512 resolution with 12 context frames), and is still several orders of magnitude faster than per-scene optimisation pipelines.

H More Results on Dynamic Scenes

H.1 Qualitative Results

We have provided video results on the DyCheck Benchmark [65] and NVIDIA Dynamic Scene Benchmark [2] on our project webpage `https://research.nvidia.com/labs/toronto-ai/bullet-timer/`. Additionally, we include novel view synthesis videos for the DAVIS dataset, DyCheck iPhone dataset, and SORA scenes. We also showcase a video demonstrating the effects of the NTE module, along with our video results on the Tanks & Temples static scenes.

H.2 Additional Quantitative Results

In this section, we compare our method with more sota models on DyCheck iPhone dataset [64] (see Tab. S5a) and NVIDIA Dynamic Scene dataset [1] (see S5b). All previous models require hours of per-scene optimization, whereas our method performs inference in real time with comparable accuracy. We also compare with DynIBaR[8] using DynIBaR's protocol, which demonstrates strong performance on the NVIDIA Dynamic Scene Benchmark(see Tab. S4). While our approach performs

Model	PSNR↑	SSIM↑	LPIPS↓
PixelNeRF [73]	20.43	0.589	0.550
GPNR [70]	24.11	0.793	0.250
AttnRend [74]	24.78	0.820	0.213
MuRF [75]	26.10	0.858	0.143
PixelSplat [15]	25.89	0.858	0.142
MVSplat [14]	26.39	0.869	0.128
GS-LRM [5]	28.10	0.892	0.114
Ours-Static	26.49	0.886	0.096
Ours-Static†	28.91	0.920	0.070
Ours-BTimer	26.82	0.891	0.089

Table S3: **Quantitative comparison of models performance on RE10K test set.** To be consistent with the baselines, we adopt the 256×256 resolution. Our Bullet Timer has been trained on both static and dynamic scenes, while the other model is only trained on RE10K training set. We highlight the best, second best and third best models. †: 4 input views.

slightly worse in terms of reconstruction quality, DynIBaR relies on extensive per-scene optimization (approximately 300 hours per NSFF sequence) and leverages additional supervision signals such as optical flow and depth. In contrast, BTimer is a fully feed-forward system: it reconstructs a scene in just one second and is trained solely with a photometric loss.

Model	PSNR↑	SSIM↑	LPIPS↓
DynIBaR [8]	30.86	0.957	0.027
Ours-BTimer	26.31	0.852	0.0730

Table S4: Quantitative comparison on NSFF benchmark using DynIBaR's protocol

I More Results on Static Datasets

We provide a comprehensive qualitative comparison of our method against the baselines, MVSplat [14] and PixelSplat [15], on the RE10K dataset, as shown in Fig. S11. For each scene, the figure also displays the input views provided to the networks. Compared to the baselines, our method produces sharper outputs and more closely aligns with the ground-truth renderings. Note that all the methods used for the evaluation in this figure are trained exclusively on RE10K. Additionally, we use two views as context for all methods to ensure fairness in evaluation and to align with the setup of the baselines. Tab. S3 presents a quantitative evaluation against the baselines under the same settings. While our static model achieves the best performance among the baselines, our dynamic *BTimer* model, trained for the dynamic task, also demonstrates strong performance on the static task, ranking third on the static benchmark.

Our complete static model, trained across all datasets, is capable of reconstructing a highly diverse set of environments. Fig. S12 showcases our model's reconstructions across a wide variety of scenes, including outdoor forward-facing, outdoor drone shots, outdoor 360-degree views, indoor 360-degree views, and indoor forward-facing scenes, as well as object-centric synthetic scenes. Notably, all these reconstructions are achieved using a shared set of weights, demonstrating that our model, trained across multiple datasets, generalizes effectively to different scenarios.

To further demonstrate the importance of training on multiple datasets for generalization to unseen datasets, we conduct an ablation study on the datasets used to train our static model. Tab. S6 compares the performance of our model when trained individually on a single dataset—RE10K, MVImageNet, DL3DV, or Objaverse—against its performance when trained on all these datasets simultaneously. The evaluation is conducted on a completely unseen dataset, the Tanks & Temples split from the InstantSplat [69] paper. Our model, whether static or dynamic, trained on all datasets significantly outperforms the single-dataset models.

Model	PSNR↑	SSIM↑	LPIPS↓
4D GS [66]	13.64	-	0.428
Gauss.Marbles [76]	16.72	-	0.413
DyBluRF [77]	17.37	0.591	0.373
D-NPC [78]	16.41	0.582	0.319
Shape-of-Motion [10]	17.32	0.598	0.296
MoSca [79]	19.32	0.706	0.264
PGDVS [39]	15.88	0.548	0.340
Depth Warp	7.81	0.201	0.678
BTimer (**Ours**)	16.52	0.570	0.338

(a)

Model	PSNR↑	LPIPS↓
D-NeRF [30]	21.49	0.232
NR-NeRF [80]	19.69	0.323
TiNeuVox [63]	19.74	0.285
NSFF [2]	24.33	0.199
MonoNeRF [6]	25.62	0.106
DynPoint [81]	26.53	0.068
D-NPC [78]	25.64	0.109
MoSca [11]	26.72	0.070
PGDVS [39]	24.41	0.186
Depth Warp	12.63	0.564
BTimer (**Ours**)	25.82	0.086

(b)

Table S5: **Additional quantitative comparisons on dynamic datasets.** (a) DyCheck iPhone dataset [64]. (b) NVIDIA Dynamic Scene dataset [1].

Figure S12: A diverse set of scenes reconstructed using our static model, trained on multiple datasets and capable of generalizing to various scenarios.

J Evaluation of Temporal Smoothness

Since our method reconstructs each timestamp individually, it is necessary to understand its temporal smoothness. In this section, we quantitatively evaluate the temporal smoothness of the reconstructed dynamic scenes, with results shown in Tab. S9. We render the reconstructed DyCheck [65] scenes from one of the evaluation fixed cameras and evaluate the rendered video using the *Temporal Flickering* metric in VBench [83]. Concretely, the metric computes the pixel-wise Mean Absolute Error in every two adjacent frames and averages over all pixels and frames:

$$S_{\text{flicker}} = \frac{1}{N}\sum_{i=1}^{N}\left(\frac{1}{T-1}\sum_{t=1}^{T-1} MAE(f_i^t, f_i^{t+1})\right), \tag{S.2}$$

where N is the number of videos, T is the number of frames per video, f_i^t is the frame t in video i, and *MAE* is the Mean Absolute Error between two consecutive frames over all pixel locations. Finally, the metric is normalized into the range of 0 to 1:

$$S_{\text{flicker-norm}} = \frac{255 - S_{flicker}}{255}. \tag{S.3}$$

The higher the metric, the less flickering will be observed in a video. BTimer achieves the second best on the Temporal Flickering metric, which suggests that our bullet-time prediction, though not explicitly associated across frames, still achieves a better temporal smoothness than other baselines that decode from some temporal representations.

Model	Datasets	PSNR↑	SSIM↑	LPIPS↓
GS-LRM* [5]	RE10K	17.56	0.546	0.310
Ours-Static	Objaverse	7.00	0.363	0.668
	MVImageNet	17.75	0.530	0.343
	DL3DV	17.92	0.566	0.278
	All Static	24.22	0.807	0.093
Ours-Full	+Dynamic	24.13	0.806	0.093

Table S6: **Baseline comparisons on the Tanks & Temples dataset (InstantSplat split).** Test views are 512×512. LPIPS are compuated on 256×256. We highlight the best, second best and third best models. *: Our reproduced results.

Method	PSNR ↑
w/o 3D Pretrain	17.94
w/ Re10K only 3D Pretrain	21.29
w/o static Co-train	22.79
w/o interpolation supervision	20.54
Full model	**24.00**

Table S7: Quantitative ablation results on NVIDIA Dynamic Scene Benchmark. Ablation models are trained with 4 context frames.

#Ctx.	Res.	Time	Mem.
4	256^2	0.02s	1.42G
12	256^2	0.15s	2.60G
12	512^2	1.55s	9.68G

Table S8: Inference cost. Model is evaluated on a single NVIDIA A100 GPU.

K Visualization of Learned Deformation

While BTimer is primarily intended for novel view synthesis at the bullet timestamp, in order to demonstrate that our model design can be also targeted for building explicit temporal correlations, we train a variant of BTimer that predicts the canonical positions (XYZ) of Gaussians instead of the pixel-aligned depths on the Objaverse4D [17] dataset. The 4 input images are taken from different camera poses and different timestamps. In Fig. S13, we render the reconstructed dynamic object from a fixed viewpoint and find that the model successfully recovers the 3D motion by predicting the positions of the Gaussians at the correctly warped locations. This is further justified by keeping only the partial reconstruction from the 3DGS associated with one of the input images, and we find out that the model learns to warp the Gaussians according to different timesteps. Canonical XYZ prediction is commonly used in object-centric cases for being bounded (LGM [72], L4GM [17]), however pixel-aligned prediction is popular in large unbounded scene for being easy to optimize (pixelSplat [15], GS-LRM [5]). Applying canonical XYZ prediction to scene data is a valuable direction that we would like to explore in future work.

L Visualization of Learned Scene Flow

Although BTimer is not trained with scene flow supervision, we show that our model effectively model scene flows under the hood in the process of learning dynamic reconstruction. We treat the Gaussian associated with each pixel in the input images as a point and treat its trajectory over time as a scene flow. The visualization in Fig. S14 suggests that the learned scene flows closely represent the actual object motion.

Model	apple	block	windmill	space	spin	teddy	wheel	Average
Ground Truth	0.9878	0.9767	0.9940	0.9939	0.9829	0.9759	0.9650	0.9823
TiNeuVox [63]	0.9807	0.9814	0.9879	0.9949	0.9832	0.9782	0.9695	0.9823
T-NeRF [64]	0.9831	0.9791	0.9866	0.9907	0.9828	0.9730	0.9624	0.9797
Nerfies [32]	0.9817	0.9791	0.9868	0.9918	0.9809	0.9720	0.9609	0.9790
HyperNeRF [4]	0.9825	0.9784	0.9865	0.9914	0.9821	0.9720	0.9584	0.9787
PGDVS [39]	0.9719	0.9738	0.9956	0.9903	0.9816	0.9649	0.9517	0.9757
BTimer (**Ours**)	0.9835	0.9760	0.9884	0.9881	0.9789	0.9746	0.9745	0.9806

Table S9: **Temporal Flickering [82] evaluation on the DyCheck [65] dataset.**. There are 7 scenes and we report their average. We highlight the best, second best and third best.

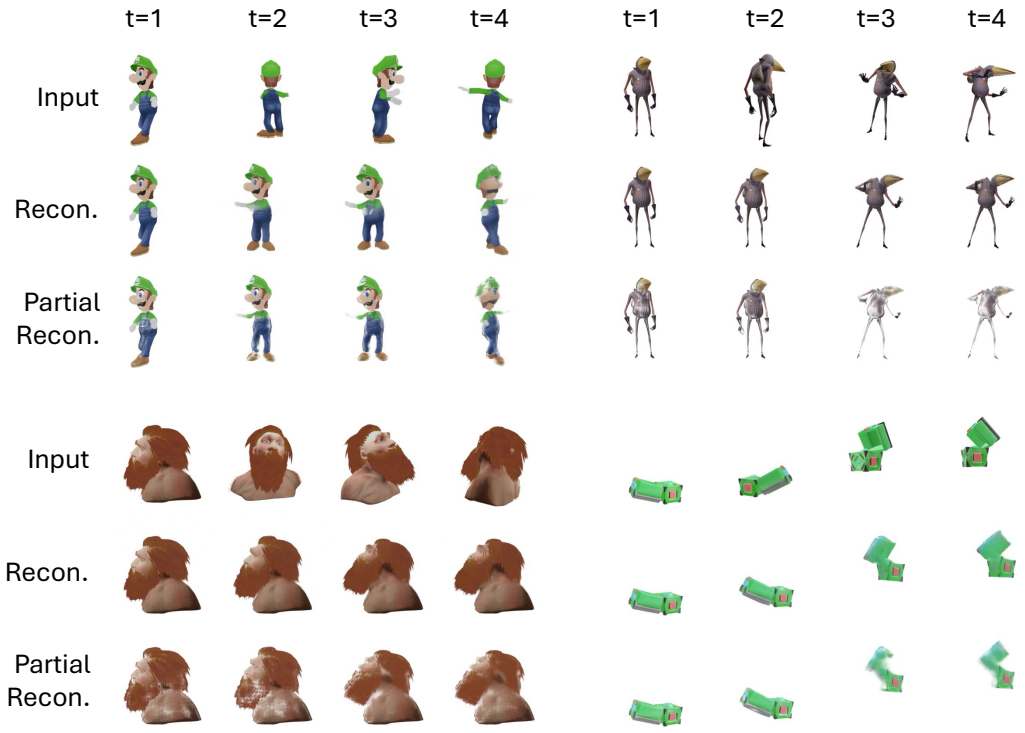

Figure S13: **Learned deformation visualization.** In each example, the first row shows the 4 input images captured from different viewpoints and timestamps, the second row is our reconstruction rendered from a fixed viewpoint, and the third row keeps only Gaussians associated from one of the input images.

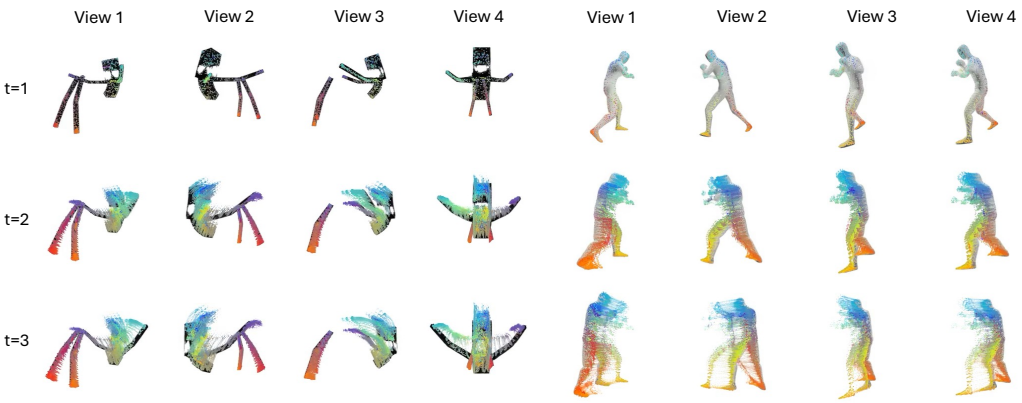

Figure S14: **Learned scene flow visualization.** We color the Gaussians by the pixel positions they associate with. As the Gaussians move, their trajectories are considered as scene flows. Our model learns meaningful scene flows that closely represent the object motion without any scene flow supervision.